

Ultrasonic attenuation in magnetic fields for superconducting states with line nodes in Sr_2RuO_4

L. Tewordt and D. Fay

I. Institut für Theoretische Physik, Universität Hamburg, Jungiusstr. 9, 20355 Hamburg, Germany
(December 2, 2024)

We calculate the ultrasonic attenuation in magnetic fields for superconducting states with line nodes vertical or horizontal relative to the RuO_2 planes. For rotating in-plane field $H(\theta)$ the attenuation $\alpha(\theta)$ exhibits variations of fourfold symmetry in the rotation angle θ . In the case of vertical nodes, the transverse T100 sound mode yields the weakest (linear) H and T dependence of α , while the longitudinal L100 mode yields a stronger (quadratic) H and T dependence. This is in strong contrast to the case of horizontal line nodes where α is the same for the T100 and L100 modes (apart from a shift of $\pi/4$ in field direction) and is roughly a quadratic function of H and T . Thus we conclude that measurements of α in in-plane magnetic fields for different in-plane sound modes may be an important tool for probing the nodal structure of the gap in Sr_2RuO_4 .

A number of experiments give evidence that the superconducting state in layered Sr_2RuO_4 ¹ consists of spin-triplet Cooper pairs with broken time-reversal symmetry. More recent experiments at low temperatures have established power law T dependence of the specific heat (T^2),² the spin-lattice relaxation rate (T^3),³ the electronic thermal conductivity,^{4,5} the penetration depth,⁶ and the ultrasonic attenuation.^{7,8} These properties are most naturally explained in terms of a spin-triplet order parameter $\mathbf{d}(\mathbf{p}) = \Delta \hat{\mathbf{z}}(p_x + ip_y)g(\mathbf{p})$ where the even-parity function $g(\mathbf{p})$ has vertical line nodes (e.g., $p_x^2 - p_y^2$ or $p_x p_y$) or horizontal line nodes [e.g., $\cos(cp_z + a_0)$] on the cylindrical Fermi surface.^{9–11} Since the measured anisotropy of the in-plane thermal conductivity $\kappa[\theta]$ for rotating in-plane magnetic field⁴ is smaller than the calculated anisotropy for vertical nodes,¹¹ and since the anisotropy of the inter-plane $\kappa[\theta]$ is insignificant,⁵ these authors have discarded vertical nodes and suggested instead horizontal nodes in the superconducting gap. Recently we have shown, however, that the amplitudes of $\kappa[\theta]$ for vertical and horizontal line nodes are about the same.¹² The small size of the observed amplitude of $\kappa[\theta]$ is due to the result that the amplitude of the variation of $\kappa[\theta]$ decreases with increasing impurity scattering and temperature. The data for ultrasonic attenuation α in Sr_2RuO_4 measured for different sound directions $\hat{\mathbf{q}}$ and polarizations $\hat{\mathbf{e}}$ in the ab plane are found to be consistent with a vertical line node structure $p_x^2 - p_y^2$ or a horizontal line of nodes in conjunction with significant gap modulation.⁷

Since the question as to the nodal structure of the superconducting gap in Sr_2RuO_4 is still unresolved, we suggest here measurements of the anisotropy of the ultrasound attenuation $\alpha(\theta)$ for rotating in-plane magnetic fields. Indeed, ultrasonic attenuation is another powerful tool for probing the anisotropic gap structure because $\alpha(\theta)$ is sensitive to the relative orientations of the sound direction and polarization, $\hat{\mathbf{q}}$ and $\hat{\mathbf{e}}$, the field $\mathbf{H}(\theta)$, and the nodal directions of the gap. We shall show that $\alpha(\theta)$ exhibits fourfold symmetric variations in rotation angle θ of the magnetic field while the variations of $\kappa[\theta]$ have twofold symmetry. It turns out that the field and temperature dependencies of α for vertical gap nodes are quite different for longitudinal and transverse sound modes while α for horizontal nodes is essentially the same for longitudinal and transverse sound modes. Thus observation of the field and temperature dependence of α for longitudinal and transverse sound modes should yield important information on the nodal structure of the gap in Sr_2RuO_4 .

Our present theory for the ultrasonic attenuation α closely follows the method for calculating the thermal conductivity in magnetic fields near H_{c2} .¹² We start with the normal and anomalous Green's functions G and F which contain both the effects of supercurrent flow and scattering by the Abrikosov vortex lattice on the quasiparticle spectrum.¹³ These Green's functions are employed in the expressions for the correlation functions for longitudinal and transverse sound propagation in the hydrodynamic regime, $\omega\tau \ll 1$, and long wavelength limit, $q\ell \ll 1$.¹⁴ Integration over the energy variable yields, in analogy to the results for κ ,¹² the following expression for the ratio of the ultrasound attenuation in the superconducting state, α_s , to that in the normal state α_n :

$$\frac{\alpha_s}{\alpha_n} = \int_0^\infty \frac{d\omega}{2T} \text{sech}^2(\omega/2T) \left\{ \int_0^{2\pi} \frac{d\phi}{2\pi} [\pi_{ij}(\phi)]^2 I(\phi) + \left[\int_0^{2\pi} \frac{d\phi}{2\pi} [\pi_{ij}(\phi)] I(\phi) \right]^2 \left[|g|^2 - \int_0^{2\pi} \frac{d\phi}{2\pi} I(\phi) \right]^{-1} \right\}, \quad (1)$$

where

$$\pi_{xx}^2(\phi) = 2 \cos^2(2\phi), \quad (\text{L100}); \quad \pi_{xy}^2(\phi) = 2 \sin^2(2\phi), \quad (\text{T100}), \quad (2)$$

$$I(\phi) = \frac{\Gamma}{\text{Im } \xi_0} \frac{[1 - \pi[\Delta\Lambda/v \sin(\phi - \theta)]^2 |f|^2 |w(z_0)|^2]}{|1 + 2[\Delta\Lambda/v \sin(\phi - \theta)]^2 |f|^2 [1 + i\sqrt{\pi} z_0 w(z_0)]|^2}, \quad (3)$$

$$z_0 = (\omega + i\gamma + \xi_0)[\Lambda/v \sin(\phi - \theta)], \quad \Lambda = (2eH)^{-1/2}, \\ \gamma = \Gamma/g, \quad g = N(\omega, H)/N_0 \quad (4)$$

Here π_{xx}^2 and π_{xy}^2 are the weight factors for the L100 (T110) and T100 (L110) sound modes^{7,10} where L = longitudinal, T = transverse, and $\hat{\mathbf{q}} \parallel [100]$ or $[110]$. We use the following notation: Γ is the normal-state impurity scattering rate, v is the in-plane Fermi velocity, $\theta = \angle(\mathbf{H}, \hat{\mathbf{a}})$ is the direction of \mathbf{H} in the ab plane, Δ^2 is the spatial average of the absolute square of the order parameter for the Abrikosov vortex lattice, and $|f(\phi)|^2$ is the normalized absolute square of the gap function. The quantity z_0 , and thus the pole ξ_0 of G , is given by the transcendental equation:^{13,12}

$$z_0 = 2(\omega + i\gamma)[\Lambda/v \sin(\phi - \theta)] + i\sqrt{\pi}[\Delta\Lambda/v \sin(\phi - \theta)]^2 |f|^2 w(z_0). \quad (5)$$

The dependencies of $(\Delta\Lambda/v)^2$ and $(\Lambda/v)^2$ on H/H_{c2} are presented in Ref. 12. The expression for ultrasonic attenuation in Eq. (1) is similar to the expression for κ in Ref. 12 apart from the missing factor ω^2 , the weight factor π_{ij}^2 instead of v_i^2 , and the vertex corrections [second term in the curly brackets in Eq. (1)]. For the vertex corrections we have used the expressions in Ref. 14 for the unitary limit $\delta_N = \pi/2$ of the phase shift for impurity scattering. In the limit $\omega \rightarrow 0$, an analytical expression for the solution $z_0 = ix_0$ of Eq. (5) is obtained which yields, in close analogy to κ ,¹² a much simpler expression for α_s/α_n in the limit $T \rightarrow 0$.

First we consider the f -wave pairing state $\mathbf{d} = \Delta \hat{\mathbf{z}}(p_x + ip_y)(p_x^2 - p_y^2)$ for which $|f|^2 = \cos^2(2\phi)$ has four vertical line nodes at $\phi = \pi/4, 3\pi/4, \dots$ on the cylindrical Fermi surface. In Fig. 1 we show our results for α_s/α_n versus H/H_{c2} for the L100 ($\theta = 0$) and T100 ($\theta = \pi/4$) modes at $T = 0$ and impurity scattering rate $\Gamma/\Delta_0 = 0.1$. Δ_0 is the BCS gap parameter, and we will always use the value $\beta_A = 1.2$ for the Abrikosov parameter. It is seen that α_s/α_n for the L100 mode exhibits a strong upward curvature near H_{c2} while it is a more linear function of H for the T100 mode. For increasing Γ/Δ_0 the upward curvatures decrease.

The solid curves for α_s/α_n in Fig. 1 are calculated by neglecting the vertex corrections in Eq. (1), while the dashed curves include the vertex corrections in the unitary impurity scattering limit. One recognizes that the effect of the vertex corrections in the unitary limit is rather small. This is also true for impurity scattering in the Born limit where $|g|^2$ in the denominator of Eq. (1) is replaced by one. It is interesting that, for field direction angles $\theta = \pi/4$ and $\theta = 0$, the vertex corrections for the L100 and T100 modes, respectively, vanish. In the following calculations and figures we shall neglect the vertex corrections.

In Fig. 2 we show the dependence of α_s/α_n on the in-plane field direction θ at $T = 0$ for fixed field strength, $\Delta\Lambda/v = 0.2$, and impurity scattering rate $\Gamma/\Delta_0 = 0.1$. One sees that $\alpha(\theta)$ has variations in θ of fourfold symmetry where the minima and maxima occur at $\theta = 0$ and $\pi/4$ for the L100 mode. For the T100 mode the maxima and minima are reversed. The maxima and minima can be explained as an effect of the ϕ dependence of the weighting factors π_{ij}^2 in Eq. (2) and the density of states since the expression $|\dots|^{-2}$ in the denominator of $I(\phi)$ in Eq. (3) is proportional to $|N(\phi, \theta)|^2$. The density of states has a minimum (maximum) for quasiparticles traveling parallel (perpendicular) to the field.¹³ The minima for L100 and T100 occur at $\theta = 0$ and $\pi/4$, respectively, because the corresponding weight factors π_{xx}^2 and π_{xy}^2 have maxima at $\theta = 0$ and $\pi/4$. For higher fields (e.g., $\Delta\Lambda/v = 0.1$) a small local maximum and two neighboring minima occur around $\theta = \pi/4$ for the T100 mode due to the node of the gap at $\theta = \pi/4$.

The sound attenuation for the other f -wave pairing state, proportional to $p_x p_y$ with $|f|^2 = \sin^2(2\phi)$, is obtained from the previous expression for $|f|^2 = \cos^2(2\phi)$ by a simple transformation, $\phi' = \phi - \pi/4$, in Eq. (1). This exchanges the results for L100 and T100 which become functions of the new field rotation angle $\theta' = \theta - \pi/4$.

We consider now the spin-triplet pairing state with horizontal line nodes⁹ where the squared gap amplitude is proportional to $|f|^2 = \cos^2(c p_z) = \cos^2[\chi]$. Then, in addition to the ϕ integration in Eq. (1), one also has to do the integration over χ from $-\pi$ to $+\pi$. In Fig. 1 we have included our result for α_s/α_n versus H/H_{c2} for the mode L100 at $T = 0$ and $\Gamma/\Delta_0 = 0.1$. A strong upward curvature occurs near H_{c2} which is similar to that of the L100 mode for vertical nodes, but is quite distinct from the almost linear dependence of α_s/α_n on H/H_{c2} for the T100 mode in the case of vertical nodes. In Fig. 2 we have plotted our results for the in-plane field variation $\alpha(\theta)$ for the L100 and T100 modes. Note that the function $\alpha(\theta)$ for T100 is obtained by shifting the function for L100 by $\theta = \pi/4$ along

the θ axis. This can be seen by a variable transformation $\phi' = \phi - \pi/4$ in Eqs. (1)–(3) making use of the fact that $|f|^2 = \cos^2(\chi)$ does not depend on ϕ . Comparison of the curves in Fig. 2 shows that the amplitudes of the variations $\alpha(\theta)$ for vertical and horizontal nodes are about the same (here about 10%). However, there is a marked difference in the form of the variations for the L100 and T100 modes for vertical nodes because, for the T100 mode, the gap node manifests itself in the structure around $\pi/4$. In contrast to this, the form of the variations for horizontal nodes is the same apart from the shift by $\pi/4$ along the θ axis.

We turn now to the ω dependence of the ϕ integrals in Eq. (1) which determine the T dependence of α_s/α_n . It is now necessary to solve Eq. (5) for z_0 as a function of $\Omega = \omega/\Delta$, and then to integrate the resulting expression for $I(\phi)$ in Eq. (3) (multiplied by $\pi_{ij}^2(\phi)$, etc.) over ϕ (and χ for horizontal nodes). We denote by $\alpha_s(\Omega)/\alpha_n$ the resulting integrand of the ω integral [without the factor $(1/2T)\text{sech}^2(\omega/2T)$]. In Fig. 3(a) we plot $\alpha_s(\Omega)/\alpha_n$ vs Ω for $|f|^2 = \cos^2(2\phi)$ for large field magnitude [$\Delta\Lambda/v = 0.2$ ($H/H_{c2} = 0.78$)] and field directions $\theta = 0$ and $\pi/4$ for both the L100 and T100 modes. It is interesting that the curves for $\theta = 0$ and $\pi/4$ cross at finite frequencies Ω which means that the minima and maxima in $\alpha(\theta)$ are interchanged. Furthermore, the Ω dependence for T100 at $\theta = \pi/4$ is almost linear while, for L100 and $\theta = 0$, it is quadratic. In Fig. 3(b) we show $\alpha_s(\Omega)/\alpha_n$ for the state $|f|^2 = \cos^2(cp_z)$.

The temperature dependence of α_s/α_n is obtained according to Eq. (1) by integrating the expression $(1/2T)\text{sech}^2(\omega/2T)\alpha_s(\Omega)/\alpha_n$ over ω . For the variable transformation from ω to $\Omega = \omega/\Delta$ we make use of the relations $\Delta/\Delta_0 = [1 - (H/H_{c2})]^{1/2}/\sqrt{\beta_A}$ and $H/H_{c2} = [1 + 6\beta_A(\Delta\Lambda/v)^2]^{-1}$.¹² In Fig. 4 we show our results for α_s/α_n vs T/T_c for vertical gap nodes at low and high field strength ($\Delta\Lambda/v = 0.6$ and 0.2 , or $H/H_{c2} = 0.28$ and 0.78) and field directions $\theta = 0$ and $\theta = \pi/4$ for the L100 and T100 modes. One recognizes that, for low T , the attenuation of the L100 mode is approximately a quadratic function of T , while it is nearly linear for the T100 mode at $\theta = \pi/4$. These different low T power laws for the L100 and T100 modes agree roughly with the results of Ref. 10 for zero field. It is interesting that the quadratic and linear T dependencies of α_s/α_n for the L100 and T100 modes correspond to the quadratic and linear dependencies of α_s/α_n on H/H_{c2} for these modes (see Fig. 1). In Fig. 4 we also show α_s/α_n vs T/T_c for the L100 mode for horizontal gap nodes and field directions $\theta = 0$ and $\pi/4$. We recall that the results for L100 for $\theta = 0$ ($\pi/4$) are identical to those for T100 for $\theta = \pi/4$ (0). One sees that the dependence on T is nearly quadratic.

In summary, we have calculated the ultrasonic attenuation α in layered Sr_2RuO_4 in the presence of in-plane magnetic fields for spin-triplet superconducting states with vertical or horizontal line nodes in the gap. For rotating in-plane field $H(\theta)$ the attenuation $\alpha(\theta)$ exhibits variations of fourfold symmetry in the rotation angle θ . At $T = 0$ the minima occur at $\theta = 0$ and $\pi/2$ for the L100 sound mode, and at $\theta = \pi/4$ and $3\pi/4$ for the T100 mode. The amplitudes of the variations are about about the same ($\approx 10\%$) for both horizontal and vertical nodes. However, in the case of vertical nodes, $\alpha(\theta)$ for the T100 mode shows characteristic structure in the directions of the nodes. For horizontal nodes the variations $\alpha(\theta)$ for the L100 and T100 modes are the same if θ is shifted by $\pi/4$. The distinction between vertical and horizontal nodes also manifests itself in the different field and temperature dependencies of α . For vertical nodes the ratio α_s/α_n exhibits a strong upward curvature as a function of H/H_{c2} near H_{c2} for the L100 mode while it is more linear for the T100 mode. In the case of horizontal nodes, the attenuation for both the L100 and T100 modes shows a strong upward curvature near H_{c2} . The temperature dependence of the sound attenuation is determined by the frequency dependence of the integrand $\alpha(\Omega)$, $\Omega = \omega/\Delta$, in the expression for α_s/α_n . It is interesting that the curves for the functions $\alpha(\Omega)$ for field directions $\theta = 0$ and $\pi/4$ cross each other twice for increasing Ω indicating that the maxima and minima are interchanged twice. This causes corresponding crossings in the T dependencies of α for the two field directions. For vertical gap nodes, at low T , α_s/α_n exhibits approximately a T^2 power law for the L100 mode and a roughly linear T dependence for the T100 mode. For horizontal gap nodes the functions α_s/α_n vs T/T_c for the L100 and T100 modes are identical for field direction differing by $\pi/4$. For low and high fields α_s/α_n follows roughly a T^2 power law.

The ultrasonic attenuation in Sr_2RuO_4 in zero field has been measured for the four in-plane modes L100, T110, T100, and L110.⁷ The attenuation follows a low temperature power law $T^{1.8}$ for the L100 (T110) mode and $T^{1.4}$ for the T100 mode. In Ref. 8 a T^2 power law below T_{imp} and a T^3 dependence above T_{imp} has been measured for the T110 mode. Calculations based on the assumption of a circular cylindrical Fermi surface and vertical gap nodes¹⁰ yield a linear T dependence of α_s/α_n for the T100 (L110) mode which disagrees with the measured $T^{1.4}$ power law and, for the L100 mode, a power law close to the measured one. The fact that the weakest T dependence occurs for the T100 mode is taken as an indication⁷ that the gap nodes point in the $[110]$ direction because this yields an excess of quasiparticles with wavevectors in this direction.

Our results for the ultrasound attenuation for vertical nodes in magnetic fields up to H_{c2} also yield the weakest (linear) H and T dependence for the T100 mode because the corresponding weight factor has a maximum in the direction of a vertical gap node. Our calculations yield a stronger (quadratic) H and T dependence for the L100 mode because the corresponding weight factor has a maximum in the direction of a vertical gap antinode. This is in strong contrast to the case of horizontal line nodes where we obtain a roughly quadratic H and T dependence for *both* the

L100 and T100 modes, which are actually identical for in-plane field directions differing by $\pi/4$.

At this point we would like to mention the modifications required if one takes the model of horizontal line nodes suggested in Ref. 7. This model can be simulated by multiplying the $\cos(cp_z)$ used in this paper (see Ref. 9) by a gap with fourfold angular modulation, $(1 + \lambda \cos 4\phi)$, $0 < \lambda < 1$, in the plane. This has the effect that the dashed curves in Fig. 2 for the variations $\alpha(\theta)$ of the L100 and T100 modes drift apart with a shift (and thus the anisotropy) that increases with increasing amplitude λ of the fourfold gap modulation. Corresponding splittings occur in the attenuation curves α versus the field (Fig. 1) and temperature (Fig. 4) for the L100 (T110) and T100 modes which are identical in our simple model of horizontal line nodes. In fact, the H and T dependencies of α for the T100 mode become weaker than those of the L100 mode for increasing amplitude λ of the gap modulation.

It should be pointed out that our theory is based on a number of simplifying assumptions. First, we have considered only the lowest order Fourier coefficient of the Green's functions with respect to the reciprocal Abrikosov vortex lattice which describes the motion of quasiparticles in the plane perpendicular to the field near H_{c2} . In addition, we have used an approximate expression for the anomalous Green's function F (see Ref. 12). An exact calculation of the correlation function has been carried out by K. Scharnberg.¹⁵ As the field decreases, the higher Fourier coefficients become more and more important and, near H_{c1} , the Doppler shift method for a single vortex becomes more appropriate. Second, we have assumed a cylindrical single sheet Fermi surface, whereas the huge anisotropy observed between the T110 and T100 normal state attenuation coefficients⁷ indicates that the anisotropy follows from the nature of the three orbitals forming the three sheets of the Fermi surface in Sr_2RuO_4 .¹⁶ These authors showed that in the case of Sr_2RuO_4 a simple viscosity tensor describing the electron-phonon interaction may not be sufficient for ultrasound attenuation. If this is the case our predictions could be changed. Third, we have assumed that the attenuation coefficients normalized to their normal state values are insensitive to the observed normal state anisotropies. Here we have taken a temperature independent scattering rate Γ giving rise to a temperature independent normal state attenuation which agrees roughly with the data for the L100 and T100 modes.⁷ Thus it cannot be excluded that the effect of the normal state anisotropy exceeds all anisotropies in the superconducting state calculated in this work.

In spite of the above uncertainties we believe that measurements of the field dependencies (in addition to the temperature dependencies) of the ultrasonic attenuation for different in-plane sound modes can still provide useful information about the nodal structure of the energy gap in Sr_2RuO_4 .

ACKNOWLEDGMENTS

We thank K. Scharnberg for helpful discussions.

-
- ¹ Y. Maeno et al., Nature (London) **372**, 532 (1994).
² S. NishiZaki, Y. Maeno, and Z. Mao, J. Low Temp. Phys. **117**, 1581 (1999); J. Phys. Soc. Jpn. **69**, 572 (2000).
³ K. Ishida et al., Phys. Rev. Lett. **84**, 5387 (2000).
⁴ K. Izawa et al., Phys. Rev. Lett. **86**, 2653 (2001).
⁵ M. A. Tanatar et al., Phys. Rev. Lett. **86**, 2649 (2001).
⁶ I. Bonalde et al., Phys. Rev. Lett. **85**, 4775 (2000).
⁷ C. Lupien et al., Phys. Rev. Lett. **86**, 5986 (2001).
⁸ H. Matsui et al., Phys. B **63**, 060505(R).
⁹ Y. Hasegawa, K. Machida, and M. Ozaki, J. Phys. Soc. Jpn. **69**, 336 (2000).
¹⁰ M. J. Graf and A. V. Balatsky, Phys. B **62**, 9697 (2001).
¹¹ T. Dahm, H. Won, and K. Maki, cond-mat/0006301 (unpublished).
¹² L. Tewordt and D. Fay, Phys. Rev. B **64**, 24528 (2001).
¹³ U. Brandt, W. Pesch, and L. Tewordt, Z. Phys. **201**, 209 (1967).
¹⁴ K. Scharnberg, D. Walker, H. Monien, L. Tewordt, and R. A. Klemm, Solid State Commun. **60**, 535 (1986).
¹⁵ K. Scharnberg, J. Low Temp. Phys. **6**, 51 (1972).
¹⁶ M. B. Walker, M. F. Smith, and K. V. Samokhin, cond-mat/0105109 (unpublished).

FIGURE CAPTIONS

1. Ultrasonic attenuation α_s/α_n vs applied field H/H_{c2} at $T = 0$ for longitudinal and transverse in-plane sound modes L100 ($\theta = 0$; $\theta = \angle(\mathbf{H}, \hat{\mathbf{a}})$) and T100 ($\theta = \pi/4$) for impurity scattering rate $\Gamma/\Delta_0 = 0.1$. Vertical gap nodes: solid and dashed curves without and with vertex corrections in the unitary impurity scattering limit, respectively. Horizontal gap nodes: dash-dot curve.

2. α_s/α_n vs $\theta = \angle(\mathbf{H}, \hat{\mathbf{a}})$ for in-plane field rotation at $T = 0$ for sound modes L100 and T100 and gap parameter $\Delta\Lambda/v = 0.2$ ($H/H_{c2} = 0.78$) and $\Gamma/\Delta_0 = 0.1$. Solid curves: vertical gap nodes. Dashed curves: horizontal gap nodes.

3. Integrand $\alpha_s(\Omega)/\alpha_n$ in Eq. (1) for α_s/α_n (without the factor $(1/2T)\text{sech}^2(\omega/2T)$) vs reduced frequency $\Omega = \omega/\Delta$ for gap parameter $\Delta\Lambda/v = 0.2$ ($H/H_{c2} = 0.78$) and field directions $\theta = 0$ (solid curves) and $\theta = \pi/4$ (dashed curves), and $\Gamma/\Delta_0 = 0.1$. (a) L100 and T100 for vertical gap nodes; (b) L100 for horizontal gap nodes.

4. α_s/α_n vs T/T_c for vL100, vT100, and hL100 (v = vertical, h = horizontal gap nodes), for field directions $\theta = 0$ (solid curves) and $\theta = \pi/4$ (dashed curves). (a) $\Delta\Lambda/v = 0.6$ ($H/H_{c2} = 0.28$), $\Gamma/\Delta_0 = 0.2$; (b) $\Delta\Lambda/v = 0.2$ ($H/H_{c2} = 0.78$), $\Gamma/\Delta_0 = 0.1$.

Fig. 1

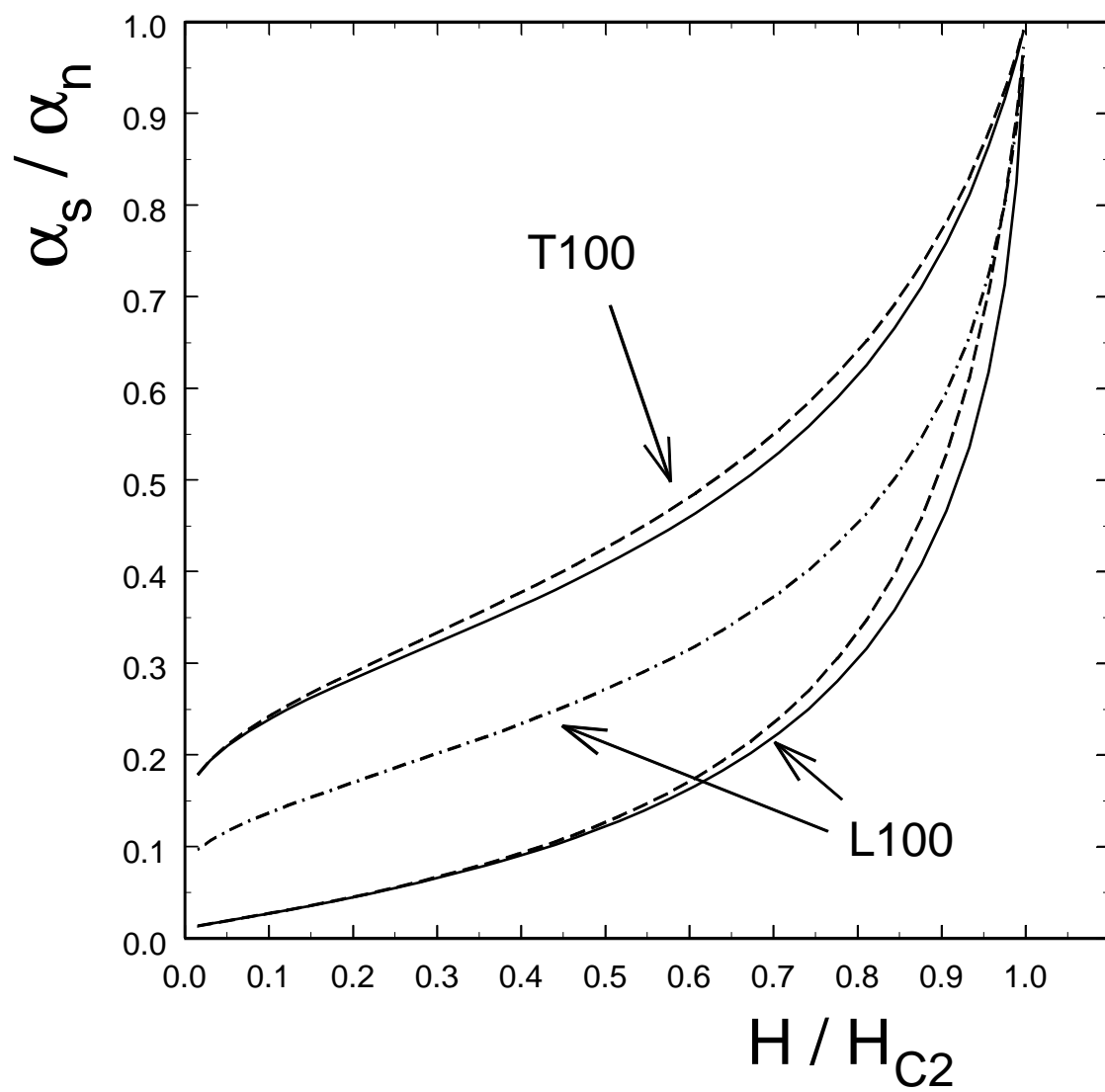
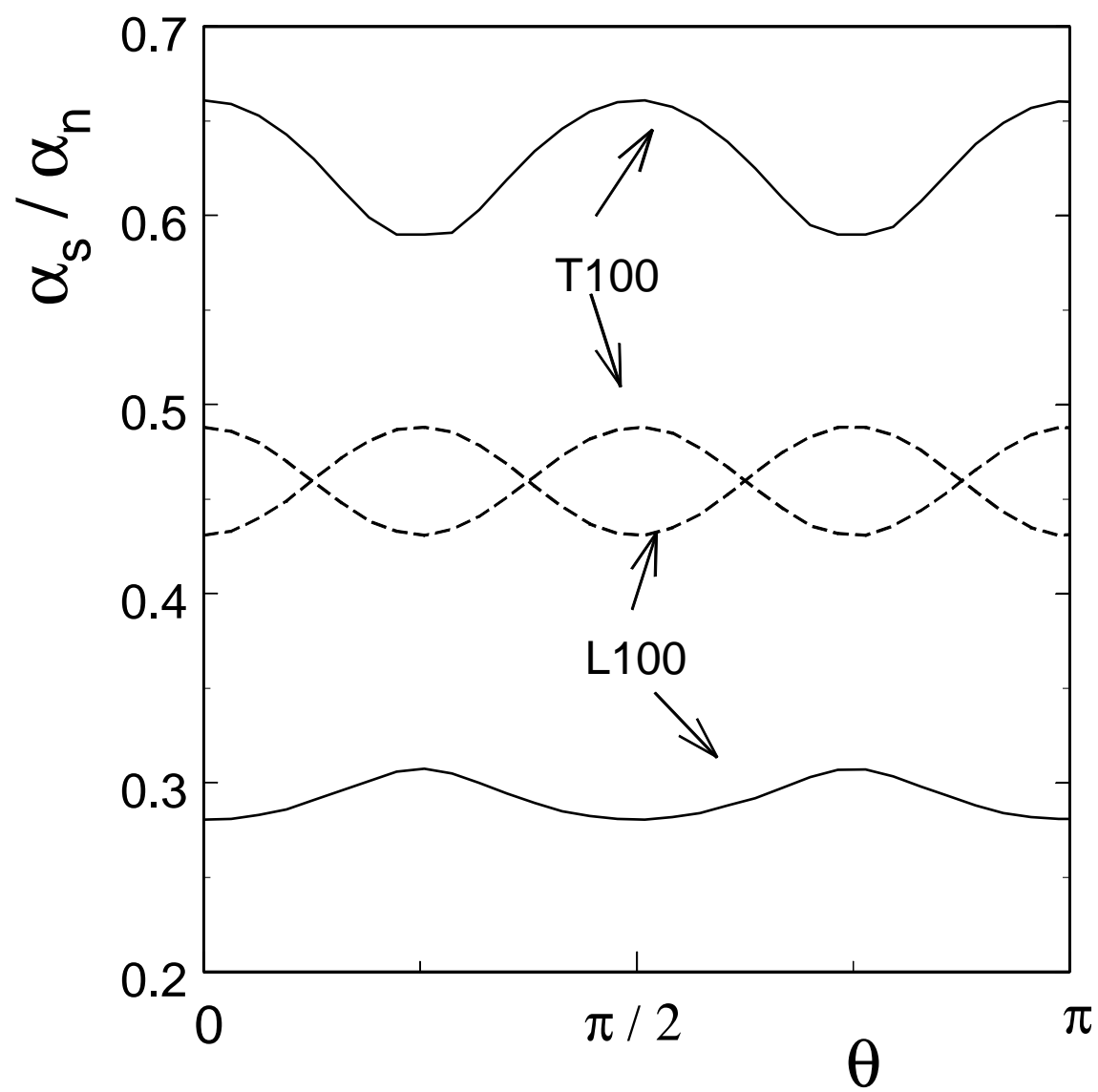


Fig. 2



Fig, 3

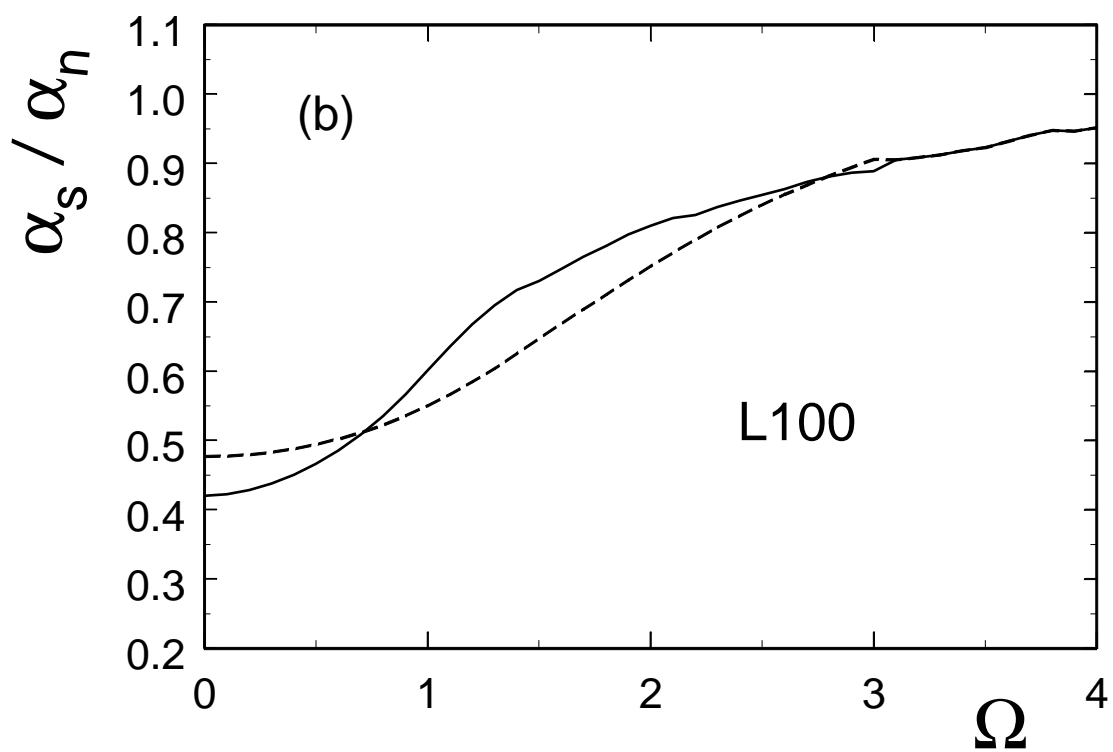
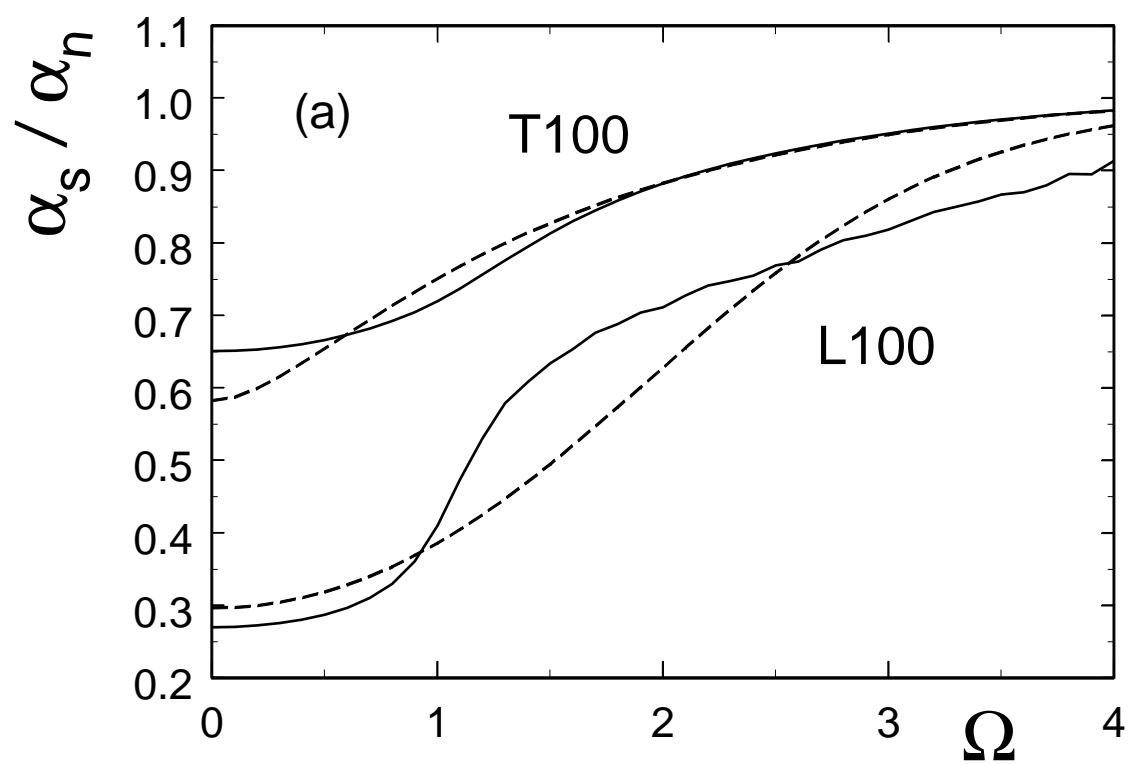


Fig. 4

